Inorganic Chemistry

Article

pubs.acs.org/IC

Importance of the Dimethylamino Functionality on a Multifunctional Framework for Regulating Metals, Amyloid-β, and Oxidative Stress in Alzheimer's Disease

Jeffrey S. Derrick,[†] Richard A. Kerr,[‡] Kyle J. Korshavn,[‡] Michael J. McLane,[‡] Juhye Kang,[†] Eunju Nam,[†] Ayyalusamy Ramamoorthy,[‡,§] Brandon T. Ruotolo,[‡] and Mi Hee Lim*[,†]

[†]Department of Chemistry, Ulsan National Institute of Science and Technology (UNIST), Ulsan 44919, Republic of Korea

[‡]Departments of Chemistry and [§]Biophysics, University of Michigan, Ann Arbor, Michigan 48109, United States

Supporting Information

ABSTRACT: The complex and multifaceted pathology of Alzheimer's disease (AD) continues to present a formidable challenge to the establishment of long-term treatment strategies. Multifunctional compounds able to modulate the reactivities of various pathological features, such as amyloid-β (Aβ) aggregation, metal ion dyshomeostasis, and oxidative stress, have emerged as a useful tactic. Recently, an incorporation approach to the rational design of multipurpose small molecules has been validated through the production of a multifunctional ligand (**ML**) as a potential chemical tool for AD. In order to further the development of more diverse and improved multifunctional reagents, essential pharmacophores must be identified. Herein, we report a series of aminoquinoline derivatives (**AQ1−4**, **AQP1−4**, and **AQDA1−3**) based on **ML**'s framework, prepared to gain a structure−reactivity understanding of **ML**'s multifunctionality in addition to tuning its metal binding affinity. Our structure−reactivity investigations have implicated the dimethylamino group as a key component for supplying the antiamyloidogenic characteristics of **ML** in both the absence and presence of metal ions. Two-dimensional NMR studies indicate that structural variations of **ML** could tune its interaction sites along the Aβ sequence. In addition, mass spectrometric analyses suggest that the ability of our aminoquinoline derivatives to regulate metal-induced Aβ aggregation may be influenced by their metal binding properties. Moreover, structural modifications to **ML** were also observed to noticeably change its metal binding affinities and metal-to-ligand stoichiometries that were shown to be linked to their antiamyloidogenic and antioxidant activities. Overall, our studies provide new insights into rational design strategies for multifunctional ligands directed at regulating metal ions, Aβ, and oxidative stress in AD and could advance the development of improved next-generation multifunctional reagents.

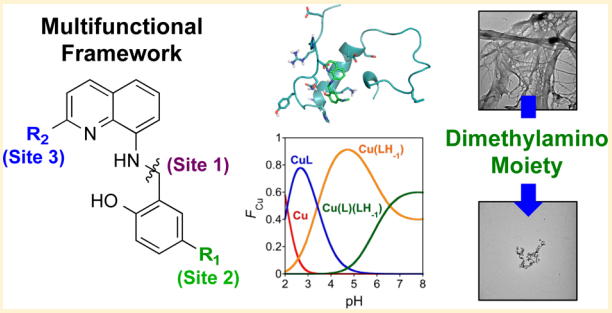

INTRODUCTION

Effective therapeutic strategies to combat Alzheimer's disease (AD), the most common form of dementia, have yet to be identified, which is most likely a result of the disease's complex and multifaceted pathology.[1−10] For example, some pathological features being actively investigated include: misfolded and aggregated proteins (i.e., amyloid-β (Aβ) and tau), metal ion dyshomeostasis and miscompartmentalization, oxidative stress, excitotoxicity, neuroinflammation, and mitochondrial damage.[1−6,11,12] Furthermore, the interconnections between many of these pathological factors, such as Aβ, metal ions, and reactive oxygen species (ROS), make the elucidation of a comprehensive molecular-level understanding of AD etiology extremely challenging.[1−4,6−9,13,14] One approach to address the inherently complex multifaceted nature of AD is to utilize multifunctional compounds able to preferentially modulate the activities of multiple targets simultaneously. This strategy has been increasing in prevalence within the literature with common targets, including Aβ, tau, various neuroreceptors (e.g., cholinergic, glutamatergic, and dopaminergic receptors), and enzymes (e.g., acetylcholinesterase, monoamine oxidase).[1,15−22] Unfortunately, a majority of the current multifunctional molecules are developed by slightly modifying existing drugs or known molecular scaffolds (e.g., tacrine, coumarin, curcumin).[1,15−22] Such a tactic is often costly and time-consuming since it frequently involves the high-throughput screening of many structural derivatives, most of which fail to be selected for further analysis.

Rather than modifying familiar frameworks, we have recently reported that novel multifunctional AD agents can be generated through the use of an incorporation approach to rational ligand design.[23,24] Initial studies with a multifunctional ligand (**ML**) identified the feasibility of designing a single molecular entity that can control metal-free and metal-induced Aβ aggregation, toxicity engendered by metal-free Aβ and metal−Aβ, and

Received: March 2, 2016

DOI: 10.1021/acs.inorgchem.6b00525
Inorg. Chem. XXXX, XXX, XXX−XXX

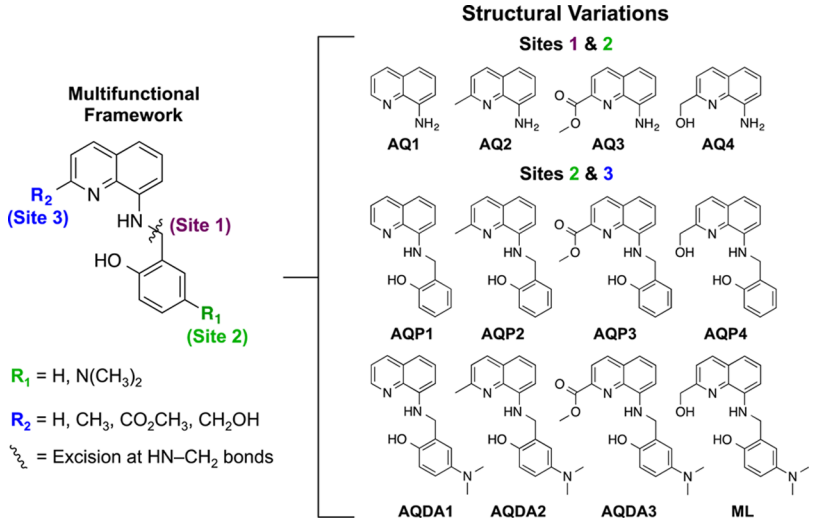

Figure 1. Structural variations on a multifunctional ligand (**ML**) framework. Modifications were performed on the multimodal scaffold to identify a structure−reactivity understanding of **ML**'s multifunctionality as well as to tune its metal binding characteristics. The quinoline portion of the structure was examined by cleavage of the HN−CH_2 bond (site 1, purple) and modulation of the functionalities at the R_2 position (site 3, blue). Furthermore, simultaneous structural alterations at the R_1 and R_2 positions (sites 2 and 3, green and blue, respectively) allowed the role of the dimethylamino group and the 4-(dimethylamino)phenol in **ML**'s activities to be illuminated.

Table 1. Values (MW, *c*log*P*, HBA, HBD, PSA, logBB, and −logP_e) of AQDA1−3 and ML[a]

Calculation	AQDA1	AQDA2	AQDA3	ML[b]	Lipinski's rules and others
MW	293	307	351	396	≤ 450
*c*log*P*	3.15	3.65	2.91	2.57	≤ 5.0
HBA	4	4	6	5	≤ 10
HBD	2	2	2	3	≤ 5
PSA	48.4	48.4	74.7	68.6	≤ 90 Å^2
logBB	−0.107	−0.323	−0.533	−0.496	< −1.0 (poorly distributed in the brain)
−logP_e	4.30 ± 0.01	4.30 ± 0.01	4.30 ± 0.01	4.50 ± 0.01	−logP_e < 5.4 (CNS+); − logP_e > 5.7 (CNS−)
CNS±prediction	CNS+	CNS+	CNS+	CNS+	CNS+; CNS−

[a]MW, molecular weight; *c*log*P*, calculated logarithm of the octanol-water partition coefficient; HBA, hydrogen bond acceptor atoms; HBD, hydrogen bond donor atoms; PSA, polar surface area; logBB = −0.0148 × PSA + 0.152 × *c*log*P* + 0.139 (logBB < −1.0 poorly distributed in the brain); −logP_e values, determined using the PAMPA-BBB assay, were calculated by the PAMPA 9 explorer software V. 3.5. Prediction of compound's ability to penetrate the central nervous system (CNS) on the basis of literature values. Compounds categorized as CNS+ possess the potential ability to penetrate the BBB while those categorized as CNS− are expected to have poor BBB permeability. [b]Reference 23.

metal-mediated ROS generation, as well as scavenge free radicals, overall validating **ML**'s structure-based design strategy.[12,23,24] Further progress toward the production of more diverse and improved multifunctional reagents is dependent on the recognition of critical pharmacophores that can be employed as figurative "building blocks" to engineer next-generation ligands through such a rational design approach. Structure−reactivity studies, using individual components within a complex molecule and structurally modified molecules, can provide the information to determine the chemical functionalities that may impart the desired reactivities.

Toward this goal, we have prepared a series of aminoquinoline (**AQ**) derivatives (i.e., **AQ1−4**, **AQP1−4**, **AQDA1−3**; Figure 1) based on the framework of **ML** in order to discern a structure−reactivity understanding of **ML**'s multifunctionality. Our *in vitro* investigations have proposed the dimethylamino functionality of **ML** to be critical toward its ability to modulate the aggregation pathways of metal-free A*β* and metal−A*β*. Two-dimensional (2D) NMR studies have shown that functionalization of the aminoquinoline moiety is capable of shifting the preferred region of interaction along the sequence of A*β*. In addition, the slight modifications to **ML**'s metal binding site are also indicated to direct the derivatives' ability to bind Cu(II) and Zn(II), control reactive oxygen species (ROS) formation, and alter Cu(II)−/Zn(II)−A*β* aggregation. The overall structural variation of **ML** also tuned its capability to scavenge free radicals. Mass spectrometric studies further illustrate the importance of the metal binding affinity of this series of small molecules in regulating metal−A*β* aggregation and potentially suggest larger, higher-order oligomers as the interacting species. Similar to **ML**, our structural derivatives are also observed to be potentially suitable in biological systems since they are moderately water soluble and potentially possess the ability to penetrate the blood-brain barrier (BBB). Overall, our studies highlight the importance of the dimethylamino moiety for imparting reactivity toward AD-relevant targets (e.g., metals, A*β*, metal−A*β*), yet further studies are still warranted to assess its transferability to other molecular scaffolds.

RESULTS AND DISCUSSION

Design Rationale and Preparation for Structural Modifications to a Multifunctional Framework. A series of aminoquinoline (**AQ**) derivatives based on our previously reported multifunctional ligand (**ML**) were generated to (i)

DOI: 10.1021/acs.inorgchem.6b00525
Inorg. Chem. XXXX, XXX, XXX−XXX

develop a structure−reactivity understanding of **ML**'s multifaceted reactivity toward metal-free Aβ, metal−Aβ, ROS, and free radicals, and (ii) reduce its relatively high binding affinity for Cu(II) and Zn(II) (i.e., dissociation constants for Cu(II) and Zn(II) in the picomolar and nanomolar range, respectively) that may potentially interfere with biologically essential metalloproteins.[23] The **AQ** derivatives were obtained by subjecting **ML** to modifications at three sites (Figure 1). First, in order to determine the significance of the phenol or 4-(dimethylamino)phenol moieties in **ML**'s activities, **AQ1−4** were prepared by excision of the HN−$(CH_3)_2$ bond (site 1, Figure 1). The role of the dimethylamino moiety in directing **ML**'s multifunctionality was also evaluated by modifying site 2 through installation of a hydrogen atom (**AQP1−4**) or a dimethylamino group (**AQDA1−4**) (Figure 1). Further modifications to the metal binding site (site 3) from a hydrogen atom (in **AQ1**, **AQP1**, and **AQDA1**) or a methyl group (in **AQ2**, **AQP2**, and **AQDA2**) to an ester (in **AQ3**, **AQP3**, and **AQDA3**) or an alcohol moiety (in **AQ4**, **AQP4**, and **ML**) allowed us to examine the difference in denticity and electronics of the ligands (Figure 1). Similar to **ML**, all **AQ** derivatives were also designed to adhere to Lipinski's rules and calculated logBB values for potential drug-likeness and BBB permeability (Table 1 and Table S1).[23,25,26]

Synthetically, the structural derivatives were obtained via synthetic routes analogous to the one previously reported for **ML**.[23,27−30] Starting from 2-methyl-8-nitroquinoline, the **AQ** derivatives, **AQ3** and **AQ4**, were produced through a multistep reaction (**AQ1** and **AQ2** were commercially available).[31] First, the nitro precursor compound, methyl 8-nitroquinoline-2-carboxylate, was prepared by bromination of 2-methyl-8-nitroquinoline followed by hydrolysis in 20% sulfuric acid to afford 8-nitroquinoline-2-carboxylic acid. 8-Nitroquinoline-2-carboxylic acid was then methylated with trimethylsilyldiazomethane (Me_3SiCHN_2), a safer alternative to diazomethane, to produce the precursor (i.e., methyl 8-nitroquinoline-2-carboxylate) to **AQ3** and **AQ4**. Hydrogenation of methyl 8-nitroquinoline-2-carboxylate in the presence of 10% palladium on carbon provided **AQ3** at a modest yield (ca. 50%). Further reduction of **AQ3** with sodium borohydride ($NaBH_4$) generated **AQ4**. The derivatives containing an aminoquinoline and phenol (i.e., **AQP1−4**) or a 4-(dimethylamino)phenol (i.e., **AQDA1−3**) were constructed by a Schiff base condensation reaction of **AQ1−4** with either salicylaldehyde (for **AQP1−3**) or 4-(dimethylamino)-2-hydroxybenzaldehyde (for **AQDA1−3**) followed by the reduction of the resultant imine with sodium triacetoxyborohydride as shown in Scheme 1.

Effects of AQ Derivatives on Metal-Free and Metal-Induced Aβ Aggregation. In order to determine the effect of structural modifications on the ability of **AQ** derivatives to modulate Aβ aggregation in both the absence and presence of metal ions [Cu(II) and Zn(II)], gel electrophoresis with Western blotting (gel/Western blot) utilizing an anti-Aβ antibody (6E10) and transmission electron microscopy (TEM) were performed to analyze the molecular weight (MW) distribution and morphological change of the resultant Aβ species, respectively. Two experiments were conducted to determine (i) the ability of the derivatives to prevent the formation of fibrillar aggregates (inhibition experiment, Figures 2a and 3a) and (ii) to dismantle preformed Aβ aggregates into smaller species (disaggregation experiment, Figures S1a and S2a). Generally, under the experimental conditions employed herein, compound-free Aβ samples with and without metal ions

Scheme 1. Synthetic Routes to AQ, AQP, and AQDA Derivatives

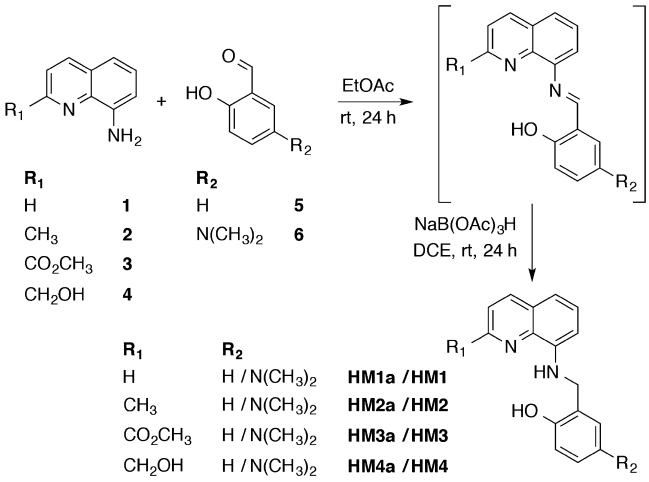

assemble into a distribution of large aggregates that are too big to penetrate into the gel matrix, which yields very little smearing in the gel/Western blots, but can be visualized via TEM.[23,31,32] The administration of compounds, capable of interacting with Aβ, inhibiting the formation of high MW aggregates, and/or disassembling preformed aggregates, typically generates a distribution of smaller-sized Aβ species that can enter into the gel and produce a substantial amount of streaking compared to the samples containing only Aβ.[23,31,32]

In the inhibition experiments, only the derivatives containing the 4-(dimethylamino)phenol moiety (i.e., **AQDA1−3**) were able to modulate the MW distribution of metal-free Aβ40 and Zn(II)−Aβ40 (Figure 2b, third column, lanes 1−3). In the case of Cu(II)−Aβ40, only one compound without the 4-(dimethylamino)phenol, **AQP1**, in addition to **AQDA1−3**, produced detectable smearing in the high MW region of the gel/Western blot (>100 kDa; Figure 2b, second column, lane 1). The reactivity of **AQP1** for Cu(II)−Aβ40 may be a result of its relatively high binding affinity for Cu(II) compared to that of the other multifunctional derivatives (*vide infra*). The inhibitory reactivity of **AQDA1−3** toward metal-free and metal-treated Aβ40 also appeared to be time dependent. Longer, darker bands (ca. 4−260 kDa) were detected on the gel/Western blot following later incubation periods (i.e., 24 h) of metal-free Aβ40 and metal−Aβ40 with **AQP1** or **AQDA1−3** (Figure 2b).

AQ derivatives also had a similar aptitude for inhibiting the self-assembly of the more aggregation-prone isoform, Aβ42.[6,11,12] Only **AQDA1−3** with the 4-(dimethylamino)-phenol functionality perturbed the MW distribution of the resultant metal-free and metal-induced Aβ42 aggregates different from that of the control samples (Figure 3b, third column, lanes 1−3). Unlike in the Aβ40 conditions, **AQP1** was not indicated to significantly ameliorate the aggregation of Cu(II)−Aβ42, which might be a result of the faster aggregation thus limiting the interaction with Cu(II) surrounded by Aβ42 (Figure 3b, second column, lane 1). TEM images of metal-free and metal-bound Aβ40 and Aβ42 samples treated with **AQDA1−3** revealed a shift from the large Aβ aggregates and fibrils found in the compound-untreated samples of metal-free and metal-bound Aβ toward morphologies that are much smaller and more amorphous (Figure 4 for Aβ42; Figure S3 for Aβ40). Consistent with the gel/Western blot findings, the

DOI: 10.1021/acs.inorgchem.6b00525
Inorg. Chem. XXXX, XXX, XXX−XXX

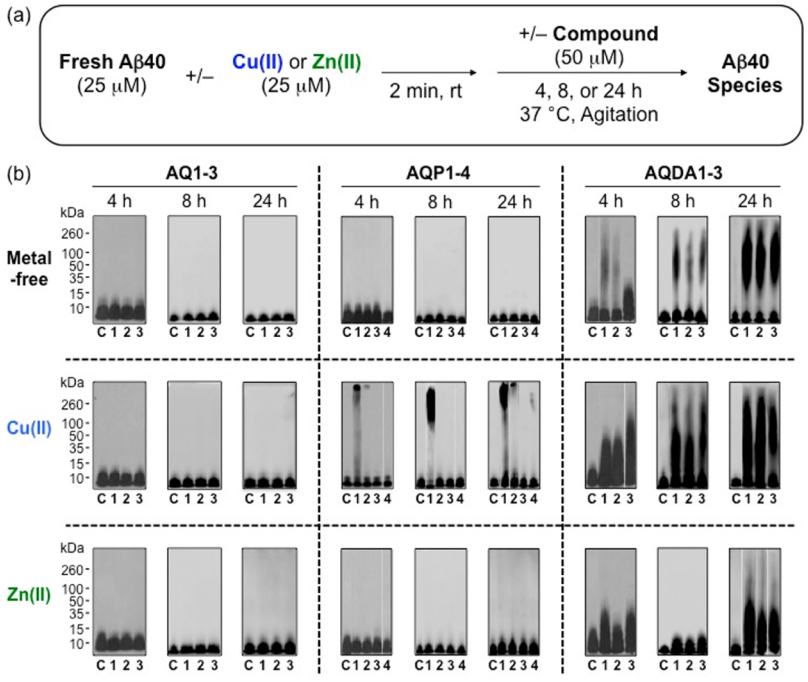

Figure 2. Ability of compounds (**AQ1**−**3**, **AQP1**−**4**, and **AQDA1**−**3**) to control the formation of Aβ40 aggregates in the absence and presence of metal ions [Cu(II) and Zn(II)]. (a) Scheme of the inhibition experiments. (b) Visualization of the resultant Aβ species from the inhibition experiments by gel/Western blot utilizing an anti-Aβ antibody (6E10). The control lane (without compound treatment) is identified by the letter C, and the lane number refers to the specific compound within each small molecule group (i.e., **AQ**, **AQP**, **AQDA**).

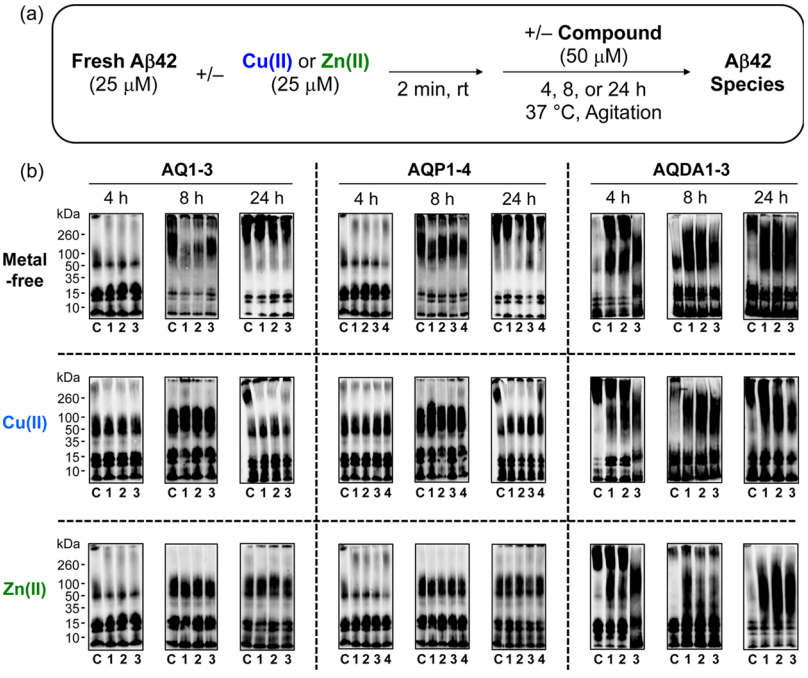

Figure 3. Capability of compounds (**AQ1**−**3**, **AQP1**−**4**, and **AQDA1**−**3**) to inhibit the formation of Aβ42 aggregates in the absence and presence of metal ions [Cu(II) and Zn(II)]. (a) Scheme of the inhibition experiments. (b) Visualization of the resultant Aβ species from the inhibition experiments by gel/Western blot utilizing an anti-Aβ antibody (6E10). The control lane (without compound treatment) is identified by the letter C, and the lane number refers to the specific compound within each small molecule group (i.e., **AQ**, **AQP**, **AQDA**).

aminoquinoline derivative, **AQ1**, and aminoquinolinephenol derivative, **AQP1**, were not observed to significantly alter the size or morphology of metal-free Aβ or Zn(II)−Aβ (Figure 4 and Figure S3). Some smaller and more unstructured aggregates, however, were identified in the Cu(II)−Aβ40 inhibition samples incubated with **AQP1** (Figure S3, middle column, inset).

We also evaluated the capacity of the multifunctional derivatives to interact with and degrade preformed Aβ40 and Aβ42 aggregates (i.e., disaggregation experiments; Figures S1a and S2a). The disaggregation experiments showed trends

DOI: 10.1021/acs.inorgchem.6b00525
Inorg. Chem. XXXX, XXX, XXX−XXX

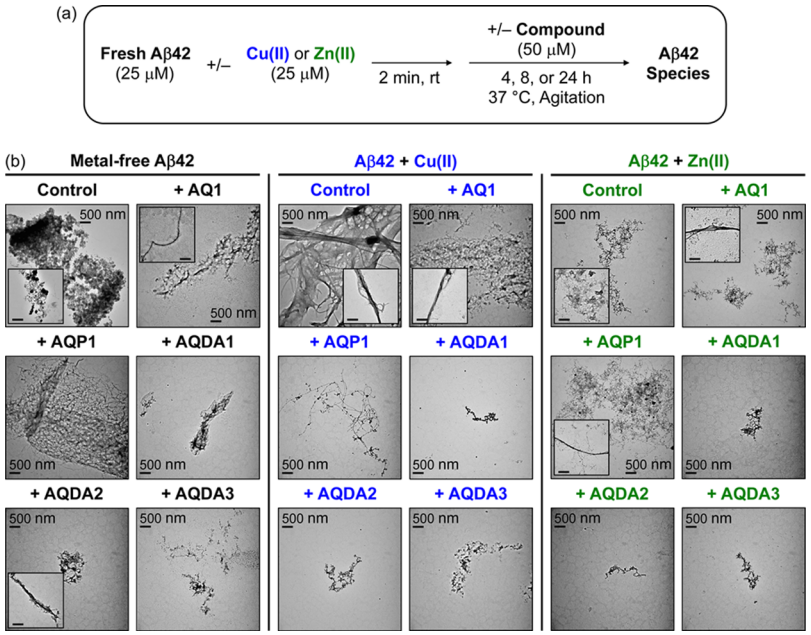

Figure 4. Morphologies of the resultant metal-free Aβ42 and metal–Aβ42 aggregates upon treatment with **AQ1**, **AQP1**, and **AQDA1–3**. (a) Scheme of the inhibition experiments. (b) TEM images for the Aβ42 samples (24 h incubation). Insets represent the minor species.

similar to those observed in the inhibition studies. Only compounds with the 4-(dimethylamino)phenol moiety (**AQDA1–3**) were able to disassemble preformed metal-free Aβ40/Aβ42 and metal–Aβ40/Aβ42 aggregates (Figures S1b, and S2b, third column, lanes 1–3). Consistent with the observations from the Cu(II)–Aβ40 inhibition experiment, **AQP1** also presented an ability to generate a distribution of smaller MW species only under Aβ40 conditions; however, the bands appeared at a higher MW region (i.e., 100–260 kDa), relative to the compounds containing the 4-(dimethylamino)-phenol moiety which produced a more disperse MW range of aggregates (i.e., ca. 4–260 kDa). Overall, our *in vitro* gel/Western blot and TEM studies suggest that the 4-(dimethylamino)phenol functionality as a critical moiety for the antiamyloidogenic properties of **ML**.

Direct Interaction between Soluble Metal-Free Aβ and AQ Derivatives. In order to elucidate the potential binding regions between Aβ40 and the **AQ** derivatives, 2D band-selective optimized flip-angle short transient heteronuclear multiple quantum coherence (SOFAST-HMQC) NMR was employed.[23,31] Chemical shift perturbation (CSP) is indicative of an altered electronic environment around the assigned residue which is likely the result of interaction with the derivatives (Figure 5 and Figure S4). Despite the various chemical alterations to the **ML** framework investigated herein, there are two primary structural regions of Aβ that show interaction with the **AQ** derivatives observed by NMR. Compounds altered either the N-terminal residues near the metal binding site of Aβ40 (i.e., predominantly E11 and V12) or the central hydrophobic residues within the self-recognition sequence (LVFFA).[7,8,11,12] It was previously demonstrated that **ML** predominantly perturbs V12 and Q15, suggesting that the N-terminal contacts may be partially responsible for its efficacy and desirable for future chemical tools.[23]

Of the **AQ** derivatives studied by NMR, both **AQ1** and **AQ2** have CSP profiles most similar to **ML** (Figure 5 and Figure S4). These molecules are not shown to have any **ML**-like antiamyloidogenic activity, which suggests that simply targeting the N-terminal metal binding site (in particular, metal binding residues H6, H13, and H14) is insufficient for such a function. Predictably, the addition of the phenol group (shown in **AQP1**, **AQP2**, and **AQP4**) shifted the preferred interaction toward the more nonpolar and aromatic residues. Of these three compounds, only **AQP4** demonstrated any interaction with N-terminal residues (E11; Figure S4d). Additionally, only **AQP1** was observed to effectively modulate Cu(II)–Aβ40 aggregation, which is likely associated with the relatively high affinity of **AQP1** for Cu(II) (*vide infra*). Combined, these results further imply that antiamyloidogenic activity is not as much a function of simply where on the monomer a compound binds but rather a function of a compound's interaction site(s) and its ability to interact with other components of the system.

The addition of the 4-(dimethylamino)phenol, instead of the phenol group, had a slightly unexpected result. While the added aromaticity promoted interactions of **AQDA1–3** with the central self-recognition sequence (like **AQP1** and **AQP2**), it also maintained contacts with more N-terminal residues (E11 and V12) by **AQDA1** and **AQDA2** which were similar to the interactions observed in both the nonreactive **AQ1** and **AQ2**, along with the functional parent, **ML** (Figure 5 and Figure S4). In addition, like **ML**, it is possible that having the slightly polar dimethylamino moiety on the framework appended to the added hydrophobicity of the phenol group remediates the shift toward hydrophobic residues seen for the **AQP** compounds. The dimethylamino functionality is indicated to be a moiety that is able to tune the interaction of hydrophobic compounds toward more polar peptide regions, functioning as a chemical rheostat. It is also coupled with consistent reactivity against Aβ. Thus, having modest hydrophilicity (in this case, instilled by the dimethylamino functionality) may promote the antiamyloidogenic activity of the compounds, as observed in both **ML** and the **AQDA** derivatives.

The interactions between Aβ and the **AQ** derivatives examined by 2D NMR were further visualized and probed by docking studies that were performed by employing AutoDock Vina[46] and the previously reported NMR structure of

DOI: 10.1021/acs.inorgchem.6b00525
Inorg. Chem. XXXX, XXX, XXX–XXX

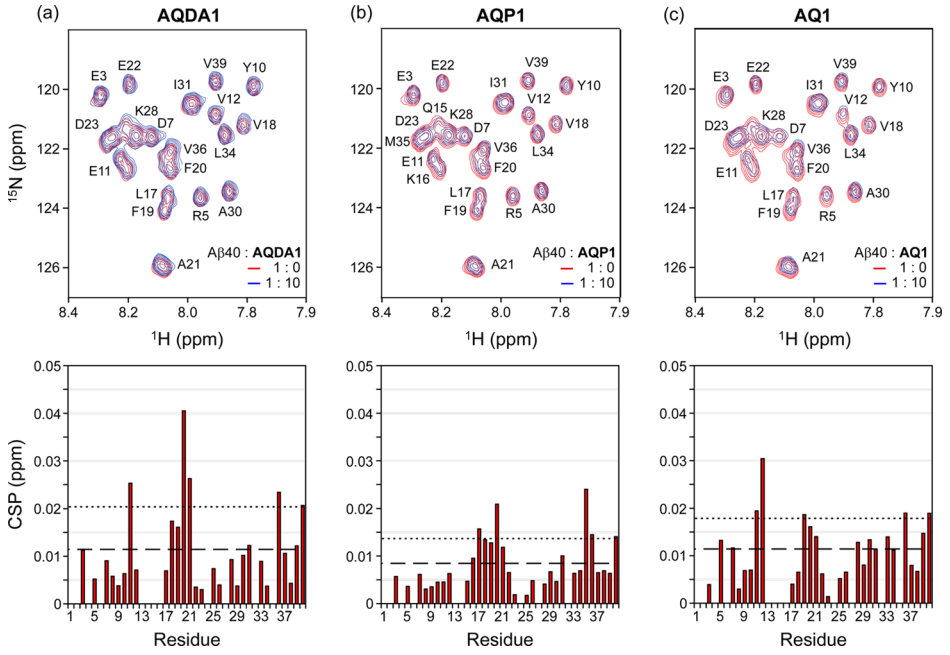

Figure 5. Interactions of **AQ1**, **AQP1**, and **AQDA1** with monomeric Aβ40, monitored by SOFAST-HMQC NMR. (a–c) SOFAST-HMQC NMR spectra (zoomed in view from 7.9 to 8.4 ppm; top) and chemical shift perturbations (CSPs) (bottom) of Aβ40 upon treatment with (a) **AQDA1**, (b) **AQP1**, or (c) **AQ1**. Two horizontal lines represent the average chemical shift (dashed line) plus one standard deviation (dotted line). Residues which show no CSP are the result of unresolved peaks in the spectra.

monomeric Aβ40 (PDB 2LFM)[43] (Figure S5). The docking results showed that, for most conformations of Aβ, the ligands bound almost exclusively in the pocket formed by the folding of the N-terminal random coil and α-helix and their adducts with the peptide were stabilized by nonspecific and/or direct intermolecular interactions (e.g., hydrogen bonding, $\pi-\pi$ stacking). These interactions had calculated binding energies ranging from −7.0 to −4.6 kcal/mol (Figure S5). Similar to the findings from our 2D NMR experiments, the **AQP** derivatives (**AQP1**, **AQP2**, and **AQP4**) containing the more hydrophobic phenol functionality were observed to penetrate more deeply into the N-terminal pocket and appeared to interact more tightly with the central self-recognition sequence. Conversely, **AQ1** and **AQ2** appeared to dock more toward the N-terminal residues while the derivatives equipped with the 4-(dimethylamino)phenol functionality (**AQDA1–3**) showed a tendency to maintain both close interactions with the N-terminal residues, mostly by hydrogen bonding, while simultaneously establishing close contacts with the α-helical central hydrophobic region. Overall, these docking findings support the 2D NMR investigations that identified the aptitude of the dimethylamino functionality to tune the interaction of hydrophobic compounds toward the N-terminal hydrophilic residues.

Analysis of AQ Derivatives Incubated with Aβ40 by Ion Mobility–Mass Spectrometry. To further explore the interactions between Aβ40 and the **AQ** derivatives studied herein, we applied nanoelectrospray–ionization mass spectrometry (nESI–MS) combined with ion mobility–mass spectrometry (IM–MS), optimized for the detection of noncovalent protein complexes.[33,34] The MS data presented in Figure 6 highlight that, among the multifunctional derivatives, only **AQP1** and **AQP4** were capable of binding Cu(II)-treated Aβ40. While no other small molecules were observed to form complexes with Cu(II)-associated Aβ40, a notable and replicable reduction in the total Cu(II)-bound Aβ species was identified upon incubation with many of the ligands studied (**AQP1**, **AQDA1**, **AQDA2**, and **ML**), when compared to the baseline levels prior to small molecule incubation supporting their metal chelation activity (Figure S6). In the absence of a source of Cu(II), no ligand binding was observed (data not shown).

To gain further insight into the structures of the complexes between Cu(II)-treated Aβ40 and the **AQ** derivatives, we measured and compared the IM arrival time distributions for these complexes (Figure 6i; see Table S2 for the supporting collisional cross section (CCS) data). Our results indicate that **AQP1** and **AQP4** binding to Cu(II)-treated Aβ leads to a distinct conformation shift when compared to the compound-untreated metal-free and metal-bound Aβ states. In particular, close analysis of the IM drift time presents a slight perturbation of the Cu(II)–Aβ40 conformations toward more expanded conformers compared to compound-free Cu(II)-associated Aβ40. These data contrast with the results for previously studied small molecules which induced conformational compaction upon coincubation with Aβ.[31,32,35] Such a difference in the conformations generated upon **AQP1** treatment (i.e., the more expanded structures compared to the compaction observed previously)[31,32,35] may suggest that **AQP1**'s ability to alter the Aβ40 aggregation pathway in the presence of Cu(II) may be directed mainly by its metal chelation properties rather than its induction of structural alteration of Aβ. A metal chelation dependence would also further validate why **AQP4** [the compound which binds Cu(II) much weaker than **AQP1** (*vide infra*)] does not modulate the aggregation of copper-bound Aβ40 *in vitro*.

On the basis of the absence of any observable Aβ–ligand complexes for the **AQ** derivatives equipped with the 4-(dimethylamino)phenol functionality (i.e., **AQDA1**, **AQDA2**, **AQDA3**), two mechanisms are proposed to rationalize the

DOI: 10.1021/acs.inorgchem.6b00525
Inorg. Chem. XXXX, XXX, XXX–XXX

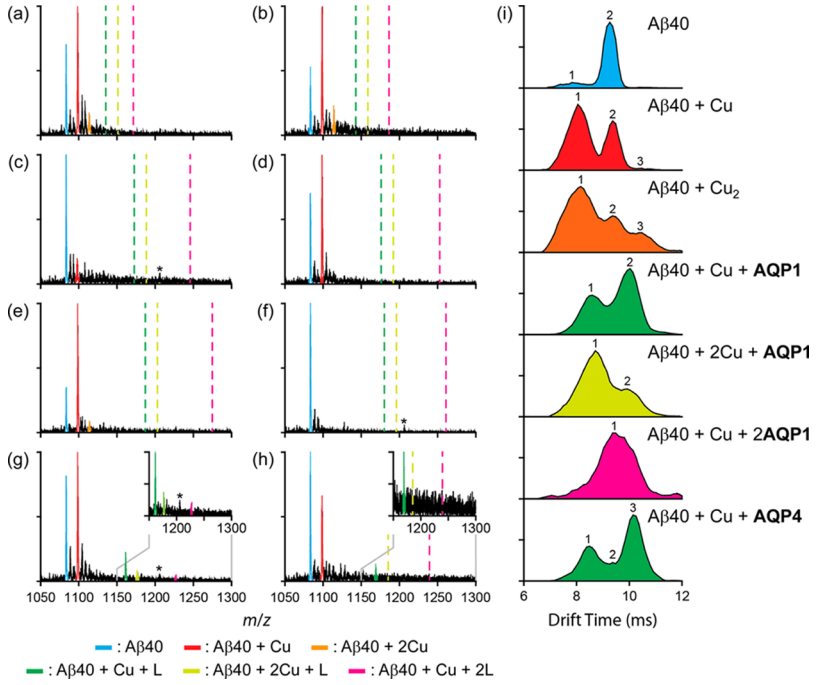

Figure 6. MS and IM–MS data for **AQ1**, **AQ4**, **AQP1**, **AQP4**, **AQDA1–3**, and **ML** upon addition of $CuCl_2$. MS spectra of (a) **AQ1**, (b) **AQ4**, (c) **AQDA1**, (d) **AQDA2**, (e) **AQDA3**, (f) **ML**, (g) **AQP1**, and (h) **AQP4**. (i) IM-MS drift time analysis. Collision cross section data for all ion mobility data sets are presented in Table S2. L = ligand (i.e., **AQ1**, **AQ4**, **AQDA1–3**, **ML**, **AQP1**, **AQP4**). Asterisk indicates a contaminant refractory to our purification methods.

activities of these molecules as Aβ modulators. First, these remaining small molecules may target larger, higher-order oligomers that are too transient for IM–MS detection under the conditions used herein. While the analyses of the interactions between small molecules, such as these, and Aβ dimers are technically possible, the presence of Cu-based salt cluster chemical noise has prevented this analysis.[35] Second, **AQDA1**, **AQDA2**, and **ML** are shown to sequester Cu(II) from Aβ, and thus our data suggests the contribution of the ligands' metal chelation properties toward its control of metal-induced Aβ aggregation.

Metal Binding Properties of AQ Derivatives. UV–visible (UV–vis) and ^{1}H NMR spectroscopy were first employed in order to probe the effects of structural modifications on the metal binding properties of the multifunctional derivatives. Upon coincubation of the ligands with increasing amounts of $CuCl_2$ or $ZnCl_2$ (Figures S7 and S8), new optical bands and/or changes in the absorbance intensity were observed. Decreases in the absorbance of the peaks at ca. 250/340 (for **AQ1**) and 250/400 nm (for **AQ3**) followed by the growth of new bands at ca. 300 and/or 450 nm (for **AQ1–3**) were discernible as $CuCl_2$ was titrated into solution (Figure S7a–c). **AQ** derivatives augmented with phenols (i.e., **AQP1–4**) produced new peaks at ca. 320 and 430 nm in the presence of $CuCl_2$ (Figure S7d–g), while the compounds with the 4-(dimethylamino)phenol moiety (i.e., **AQDA1–3**) generated new optical bands at ca. 380 and 470 nm (Figure S7h–j).

Administration of $ZnCl_2$ into solutions of **AQ** derivatives resulted in less noticeable spectral changes when compared to the $CuCl_2$ results (Figure S8). Optical shifts from ca. 350 to 300 nm were detected upon increased addition of $ZnCl_2$ to solutions of **AQ1** and **AQ2** (Figure S8a,b). Incubation of **AQP1**, **AQP2**, and **AQP4** with $ZnCl_2$ caused various spectral changes at ca. 250, 300, and 350 nm (Figure S8d,e,g). Similar to the $CuCl_2$ experiments, the $ZnCl_2$ binding peaks for the derivatives containing the 4-(dimethylamino)phenol functionality were relatively red shifted compared to the **AQP** derivatives (i.e., new peaks growing in at ca. 350 and 450 nm; Figure S8h–j). No significant changes in the UV–vis spectra could be identified for **AQ3** and **AQP3** under the experimental conditions employed; therefore, ^{1}H NMR spectroscopy was utilized to further probe their Zn(II) binding. Introduction of 3.5 equiv of $ZnCl_2$ to a CD_3CN solution of **AQ3** induced a slight downfield chemical shift of the quinoline protons, demonstrating the potential involvement of the nitrogen donor atoms from the primary amine and quinoline ring in Zn(II) coordination (Figure S9). No significant chemical shifts were observed when $ZnCl_2$ was added to a solution of **AQP3**; however, this is most likely a result of its limited solubility under the experimental conditions. Overall, our UV–vis and NMR studies indicate the ability of the structural derivatives of **ML** to bind both Cu(II) and Zn(II).

In order to comprehend the solution speciation of the **AQ** derivatives in the absence and presence of Cu(II) and attempt to determine the effects of structural variations on the Cu(II) binding affinity of our ligands, UV–vis variable-pH titration experiments were conducted. First, spectrophotometric titrations of the ligands (i.e., **AQP1**, **AQP4**, **AQDA1–3**) were used to estimate the acidity constants (pK_a) [see Figure S10; for **AQP1**, pK_{a2} = 3.67(4), pK_{a3} = 9.92(6); for **AQP4**, pK_{a2} = 3.78(8), pK_{a3} = 10.11(8); for **AQDA1**, pK_{a1} = 3.72(9), pK_{a2} = 6.61(5), pK_{a3} = 8.99(6); for **AQDA2**, pK_{a1} = 3.21(9), pK_{a2} = 4.82(6), pK_{a3} = 7.69(4); for **AQDA3**, pK_{a1} = 2.30(8), pK_{a2} = 3.82(3), pK_{a3} = 6.73(5)]. The solution speciation diagrams depict the presence of three species for the phenol derivatives, **AQP1** and **AQP4** (anionic, neutral, and monoprotonated species; LH_{-1}, L, and LH), and predict the neutral ligand (L) predominantly being present at physiological pH (i.e., 7.4;

DOI: 10.1021/acs.inorgchem.6b00525
Inorg. Chem. XXXX, XXX, XXX–XXX

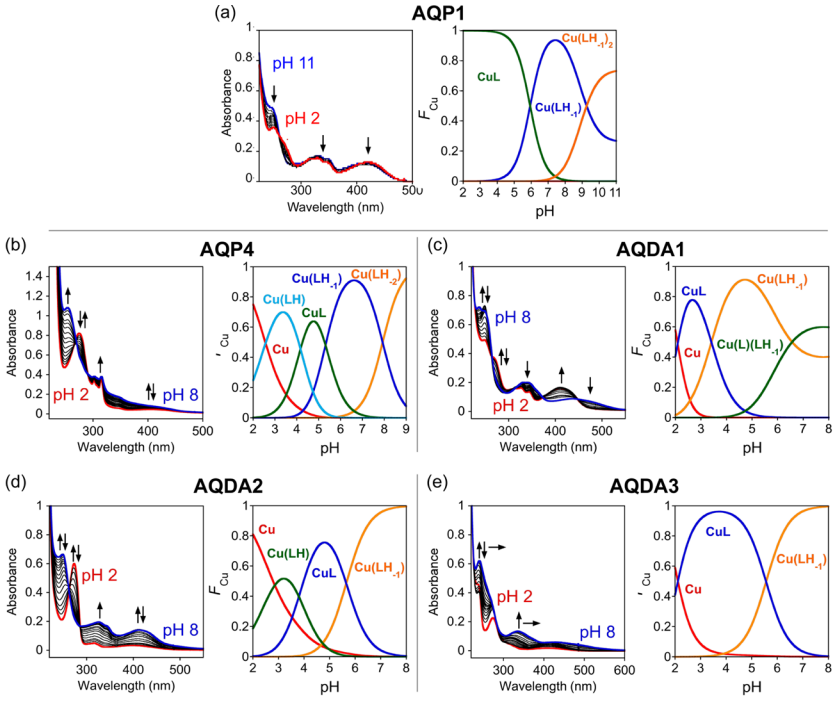

			logβ^a				
		L =	**AQP1**	**AQP4**	**AQDA1**	**AQDA2**	**AQDA3**
Cu + L + LH_{-1}	⇌	Cu(L)(LH_{-1})	—	—	30.98(9)	—	—
Cu + $2LH_{-1}$	⇌	Cu(LH_{-1})$_2$	17.82(1)	—	—	—	—
Cu + LH_{-2}	⇌	Cu(LH_{-2})	—	-1.97(8)	—	—	—
Cu + LH_{-1}	⇌	Cu(LH_{-1})	13.95(4)	5.94(7)	16.47(1)	8.32(2)	8.00(7)
Cu + L	⇌	CuL	19.89(2)	11.25(7)	19.88(1)	13.97(5)	13.57(3)
Cu + LH	⇌	Cu(LH)	—	15.42(6)	—	17.77(4)	—
pCu (= $-\log[Cu_{unchelated}]$; pH 6.6 / 7.4)			10.78 / 11.44	9.11 / 10.88	13.80 / 14.80	7.25 / 7.85	7.68 / 7.93

Figure 7. Solution speciation studies of **AQP1**, **AQP4**, and **AQDA1**−**3** in the presence of Cu(II). UV−vis variable-pH titration spectra (left) and solution speciation diagrams (right) of (a) **AQP1**, (b) **AQP4**, (c) **AQDA1**, (d) **AQDA2**, and (e) **AQDA3** upon incubation with Cu(II) (F_{Cu} = fraction of species at given pH). Stability constants (logβ) of Cu(II)−L complexes (L = **AQP1**, **AQP4**, and **AQDA1**−**3**) are summarized in the table. Charges are omitted for clarity. [a]The error in the last digit is shown in parentheses.

Figure S10a,b). Due to the protonation of the dimethylamino group, **AQDA** derivatives contain an additional diprotonated species (LH_2) in the pH range examined and exist in a mixture of neutral and cationic (for **AQDA1**) or anionic and neutral (for **AQDA2** and **AQDA3**) species (Figure S10c−e). Overall, the relative abundance of the neutral form of the ligands at pH 7.4 (ca. 100% for **AQP1** and **AQP4**; ca. 50% for **AQDA1**−**3**) may explain their potential BBB permeability, as suggested by Lipinski's rules, the PAMPA-BBB assay, and calculated logBB values (Table 1 and Table S1).

Once pK_a values were obtained for the ligands of interest, solution speciation experiments in the presence of $CuCl_2$ were carried out to determine if structural modifications to **ML**'s framework at sites 2 and 3 could alter its high apparent dissociation constant for Cu(II) (picomolar K_d at pH 7.4), while still maintaining competitive metal binding with Aβ (e.g., nanomolar range).[7,9,11,12,23] On the basis of the stability constants (logβ) and values of pCu (pCu ≈ $-\log[Cu_{unchelated}]$) (Figure 7), the approximate dissociation constants (K_d = $[Cu_{unchelated}]$) for the multifunctional derivatives were determined. As summarized in the table in Figure 7, the more inert Cu(II)−ligand complexes were shown in the order of **AQDA1**, **AQP1**, **AQP4**, **AQDA3**, and **AQDA2**. Interestingly, the tridentate ligands, **AQDA1** and **AQP1**, with hydrogen atoms in the R_2 position, presented the strongest affinity for Cu(II) compared to the other tetradentate ligands measured herein (i.e., **AQP4**, **AQDA3**), thus possibly explaining the ability of **AQP1** to modulate the aggregation of Cu(II)−Aβ40 (Figure 2 and Figure S1). This trend may be explained by the ability of **AQDA1** and **AQP1** to form 1:2 complexes [Cu(II):ligand] in addition to the 1:1 stoichiometry observed for the other derivatives (Figure 7a,c).[27] Comparison of the apparent K_d values of **AQDA1** with **AQP1** and **ML** with **AQP4** indicates that the dimethylamino functionality slightly increases the metal binding affinity, as would be expected with the installation of a electron donating group located *para* to the oxygen donor atom of the phenol. **AQDA2** and **AQDA3** were determined to have larger K_d values [lower binding affinity for Cu(II)] than **ML**. The slightly smaller K_d of **AQDA3** for Cu(II), compared to **AQDA2**, is most likely due to the weak contribution from the ester functionality. Overall, tuning metal binding strengths of the multifunctional derivatives is able to be accomplished through structural modifications at the R_1 and R_2 positions.

Competition reactions, monitored by UV−vis, were also conducted to examine the selectivity of **AQP4** and **AQDA1**−**3** for Cu(II) over other biologically relevant divalent metal ions (i.e., Mg(II), Ca(II), Mn(II), Fe(II), Co(II), Ni(II), Zn(II)). As

DOI: 10.1021/acs.inorgchem.6b00525
Inorg. Chem. XXXX, XXX, XXX−XXX

shown in Figure S11, in the presence of equimolar (Figure S11a) or excess metal ions (20 equiv; Figure S11b), the ligands still exhibited spectral changes consistent with the formation of Cu(II) complexes. Fe(II) did appear to competitively interact with **AQP4**, **AQDA1**, and **AQDA2**, especially at excess concentrations. It is also worth noting that the exact quantification of the selectivity for Cu(II) over Ni(II) and Zn(II) for **AQP4** and Co(II) for **AQDA1** could not be determined due to the optical overlap of their respective metal binding bands, but the overall spectral changes were suggestive of preferential binding to Cu(II) (Figure S11). Collectively, these results present that **AQ** derivatives can competitively bind to Cu(II) over other biologically available divalent metal ions and that their metal affinities can be modulated through structural modifications.

Biological Properties: ROS Formation Control, Free Radical Scavenging Capacity, and Cytotoxicity. The extent to which structural modifications affect the biological properties of our multifunctional derivatives was also investigated. The ability to control the redox cycling between Cu(I) and Cu(II) in order to reduce ROS production through Fenton-like chemistry was first analyzed by the 2-deoxyribose assay which measures the capacity of ligands to control the formation of copper-catalyzed hydroxyl radicals.[23,36] As depicted in Figure 8a, copper-mediated generation of hydroxyl

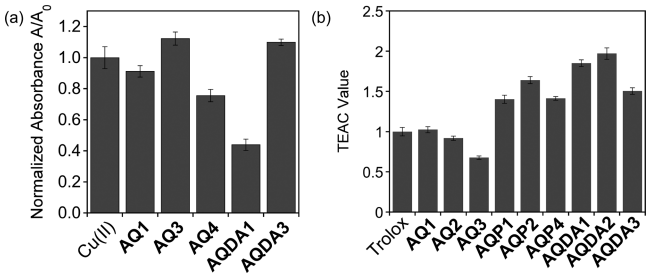

Figure 8. Biological activities of small molecules. (a) Inhibitory activity of **AQ1**, **AQ3**, **AQ4**, **AQDA1**, and **AQDA3** toward Cu-mediated ROS formation as determined by the 2-deoxyribose assay. The absorbance values are normalized to the ligand-free condition ([$CuCl_2$] = 10 μM; [ligand] = 125 μM). (b) Antioxidant activity of **AQ1**−**3**, **AQP1**, **AQP2**, **AQP4**, and **AQDA1**−**3**, identified by the TEAC assay using cell lysates. The TEAC values are relative to that of the vitamin E analogue, Trolox (6-hydroxy-2,5,7,8-tetramethylchroman-2-carboxylic acid).

radicals was most significantly reduced upon treatment with **AQDA1**. Relative to **AQDA1**, the other derivatives evaluated showed very little aptitude to attenuate hydroxyl radical formation, possibly due to their metal binding properties, including weaker binding affinity for Cu(II) compared that of **AQDA1** or **ML**. Still, **ML** appeared to be about twice as efficient at controlling the formation of hydroxyl radicals relative to **AQDA1** (A/A_0 of ca. 0.40 for **AQDA1**; A/A_0 of ca. 0.20 for **ML**).[23] The enhanced ROS formation control of **ML** is most likely due to its tetradentate metal binding center which can easily accommodate the preferred square planar geometry of Cu(II) but prohibit the generation of linear or tetrahedral geometries favored by Cu(I). In fact, on the basis of crystallographic data reported for **AQP1**, **AQDA1** may be able to facilitate a tetrahedral copper-binding mode depending on the metal-to-ligand stoichiometry and the pH of the solution.[27]

In order to evaluate the antioxidant capacity of the **AQ** derivatives, the Trolox equivalent antioxidant capacity (TEAC) assay which measures the ability of the multifunctional derivatives to quench preformed ABTS cation radicals ($ABTS^{\bullet+}$; ABTS = 2,2′-azino-bis(3-ethylbenzothiazoline-6-sulfonic acid)[15,37] was performed using lysates of human neuroblastoma SK-N-BE(2)-M17 cells. Cell lysates were utilized in order to get a more accurate measure of the antioxidant capacity of the **AQ** derivatives in a more biologically relevant heterogeneous environment. As shown in Figure 8b, the compounds containing the phenol or 4-(dimethylamino)-phenol functionalities were able to scavenge free radicals about two times more effectively than that of the water-soluble vitamin E analogue, Trolox. These findings are in-line with the known antioxidant properties of phenols.[38−40] The most efficient antioxidants, **AQDA1** and **AQDA2**, were still less active than **ML** which was determined to be ca. 2.5 times as effective as Trolox,[23] indicating that the primary alcohol in the R_2 position may contribute to the antioxidant activity of **ML**. In addition, an ester at the R_2 site appeared to reduce both the abilities of the compounds to control ROS generation and scavenge free radicals relative to those of the other multifunctional derivatives (Figure 8a,b).

Finally, the MTT assay [MTT = 3-(4,5-dimethyl-2-thiazolyl)-2,5-diphenyl-2*H*-tetrazolium bromide] was employed to evaluate the toxicity of the **AQ** derivatives in the mouse Neuro-2a (N2a) neuroblastoma cell line with and without $CuCl_2$ and $ZnCl_2$ (Figures S12). Cell viability of ca. 80% was measured for N2a cells treated with 5 μM of the **AQ** derivatives in the absence and presence of metal ions ($CuCl_2$ or $ZnCl_2$) (Figure S12a,b). A little more fluctuation in cell viability was observed upon increasing the concentration of compound to 10 μM with and without metal ions, but still most derivatives appeared to retain values around ca. 75−85% (Figure S12c,d). In particular, with the exception of **ML**, the multifunctional derivatives containing the 4-(dimethylamino)phenol functionality are indicated to be relatively more cytotoxic. Overall, our cell studies suggest that the structural variations in the framework may also trigger its differing levels of toxicity in living cells.

CONCLUSION

A series of derivatives, **AQ1**−**4**, **AQP1**−**4**, and **AQDA1**−**3**, was developed based on the structural framework of the multifunctional ligand, **ML**, in order to tune its affinity for Cu(II) and to establish a structure−reactivity understanding of **ML**'s activities to modulate metal-free and metal-bound Aβ aggregation, control metal-mediated ROS formation, and scavenge free radicals. Only compounds augmented with the dimethylamino functionality displayed noticeable modulation of both metal-free and metal-treated Aβ aggregation *in vitro*, with the exception of **AQP1** which exhibited its ability to regulate the aggregation of Cu(II)−Aβ40, which was most likely aided by its metal chelating properties (i.e., pCu = 11.44 at pH 7.4). On the basis of NMR investigations, this dimethylamino moiety appears to act to control the distribution of the compounds' interaction with the N-terminal metal binding region and/or the central self-recognition sequence of Aβ40. **ML** was previously found to preferentially target the polar N-terminal residues, which suggests that the dimethylamino group is at least partly responsible for Aβ interaction.[23] Favoring these interactions may be important for directing the formation of stable ternary complexes of Aβ−metal−ligand. Under our MS

DOI: 10.1021/acs.inorgchem.6b00525
Inorg. Chem. XXXX, XXX, XXX−XXX

and IM−MS conditions, only noncovalent interactions between Aβ and **AQP1** or **AQP4** when Cu(II) was present with slight structural elongation were observed, rather than compaction of the peptide which has been previously reported for other inhibitors.[31,32,35] Preferential transient interactions with higher-order oligomers that cannot easily be detected by IM−MS may explain the absence of complexation peaks in the **AQDA1−3**-treated samples that most noticeably perturbed metal-free and metal-treated Aβ aggregation *in vitro*. Structural modifications to **ML** also had drastic effects on its metal binding properties, ROS formation control, and free radical scavenging capacity. Substitution of the primary alcohol on **ML** with a hydrogen atom allowed for the formation of 1:1 and 1:2 (metal:ligand) complexes, providing a higher binding affinity for Cu(II) with respect to the other **AQ** derivatives. Structural variations also had impacts on compounds' abilities to control ROS formation and scavenge free radicals. **AQDA1**, with a hydrogen atom at the R_2 site, was indicated to be the most efficient at controlling the generation of hydroxyl radicals, while the compounds containing the phenol or 4-(dimethylamino)phenol groups (**AQP1−4** or **AQDA1−3** and **ML**) were much more potent antioxidants with respect to their **AQ** counterparts (**AQ1−4**). Conversely, the endowment with an ester, shown in **AQ3**, **AQP3**, or **AQDA3**, appeared to negatively alter the capacity to inhibit ROS generation and scavenge free radicals. Overall, by employing a series of **AQ** derivatives, a relationship between structures of the small molecules and reactivities toward targets found in AD (e.g., metal-free Aβ/metal−Aβ, metals, ROS) was established. These structure−reactivity insights, gleaned through our studies, may aid in further design of more sophisticated multifunctional ligands, especially once the degree of transferability of these studies has been determined.

EXPERIMENTAL SECTION

Materials and Methods. All reagents were purchased from commercial suppliers and used as received unless otherwise noted. Aβ40 and Aβ42 were purchased from Anaspec (Aβ42 = DAEFRHDSGYEVHHQKLVFFAEDVGSNKGAIIGLMVGGVVIA; Fremont, CA). NMR and mass spectrometric analysis of small molecules were conducted on a 400 MHz Varian NMR spectrometer and a Micromass LCT electrospray time-of-flight (TOF) mass spectrometer, respectively. Trace metal contamination was removed from buffers and solutions used for metal binding and Aβ experiments (*vide infra*) by treating with Chelex overnight (Sigma-Aldrich, St. Louis, MO). Optical spectra were recorded on an Agilent 8453 UV−visible (UV−vis) spectrophotometer. TEM images were taken using a JEOL JEM-2100 transmission electron microscope (UNIST Central Research Facilities, Ulsan National Institute of Science and Technology, Ulsan, Republic of Korea). Absorbance values for biological assays, including cell viability assay, PAMPA-BBB, 2-deoxyribose assay, and TEAC assay, were measured on a Molecular Devices SpectraMax 190 microplate reader (Sunnyvale, CA). Ion mobility-mass spectrometry experiments investigating the interaction of **AQ** derivatives with Aβ in the absence and presence of Cu(II) were acquired using a quadrupole-ion mobility-TOF (Q-IM-TOF) mass spectrometer (Waters Synapt G2, Milford, MA) equipped with a nanoelectrospray ionization (nESI) source. NMR studies of small molecules with Aβ were performed on a 600 MHz Bruker NMR spectrometer (University of Michigan, Ann Arbor, MI).

Syntheses. The compounds, quinolin-8-amine (**AQ1**) and 2-methylquinolin-8-amine (**AQ2**), were purchased from TCI chemicals. 5-(Dimethylamino)-2-hydroxybenzaldehyde (**DHB**),[28] methyl 8-aminoquinoline-2-carboxylate (**AQ3**),[29,31] (8-aminoquinolin-2-yl)-methanol (**AQ4**),[29,31] 2-((quinolin-8-ylamino)methyl)phenol (**AQP1**),[29,30] and 4-(dimethylamino)-2-(((2-(hydroxymethyl)-quinolin-8-yl)amino)methyl)phenol (**ML**)[23] were prepared by adapting previously reported methods.

2-(((2-Methylquinolin-8-yl)amino)methyl)phenol (AQP2). To a solution of dry ethyl acetate (16 mL) was added 2-methylquinolin-8-amine (**AQ2**) (300 mg, 1.89 mmol). Salicylaldehyde (198 μL, 1.89 mmol) was slowly added to the reaction mixture. The reaction mixture was then protected from the light and allowed to stir overnight for 24 h. After 24 h, the reaction mixture was concentrated and dried. To a solution of dichloroethane (DCE) (16 mL) was added sodium triacetoxyborohydride (804 mg, 3.78 mmol). The sodium triacetoxyborohydride solution was then slowly added to the dried reaction mixture and allowed to stir for 48 h (protected from the light). After 48 h, the reaction mixture was concentrated and purified by column chromatography (Al_2O_3, 1:10 ethyl acetate (EtOAc)/hexanes (Hx), R_f = 0.23) to yield the final product (light yellow powder, 241 mg, 0.912 mmol, 48%). ^{1}H NMR (400 MHz, $(CD_3)_2SO$)/δ (ppm): 2.62 (3H, s), 4.41 (2H, d, J = 4.0 Hz), 6.57 (1H, d, J = 8.0 Hz), 6.68 (2H, m), 6.81 (1H, d, J = 8.0 Hz), 6.96 (1H, d, J = 8.0 Hz), 7.03 (1H, t, J = 8.0 Hz), 7.18 (2H, m), 7.34 (1H, d, J = 8.0 Hz), 8.05 (1H, d, J = 8.0), 9.07 (1H, s). ^{13}C NMR (100 MHz, $(CD_3)_2SO$)/δ (ppm): 25.3, 42.1, 105.2, 113.6, 115.4, 119.2, 122.7, 125.7, 126.7, 127.1, 128.2, 136.6, 137.3, 144.2, 155.6, 155.7. HRMS Calcd for $C_{17}H_{17}N_2O$ $[M + H]^+$, 265.1341; found 256.1331.

Methyl 8-((2-hydroxybenzyl)amino)quinoline-2-carboxylate (AQP3). A solution of methyl 8-aminoquinoline-2-carboxylate (**AQ3**) (100 mg, 0.494 mmol) was utilized to prepare **AQP3** following a procedure identical to the one described for **AQP2**. **AQP3** was purified by column chromatography (SiO_2, 1:5 EtOAc/dichloromethane (DCM), R_f = 0.72) to yield the final product (yellow-orange powder, 79.3 mg, 0.257 mmol, 52%). ^{1}H NMR (400 MHz, $(CD_3)_2SO$)/δ (ppm): 3.91 (3H, s), 4.46 (2H, s), 6.67−6.70 (2H, m), 6.82 (1H, d, J = 8.0 Hz), 7.02 (1H, t, J = 8.0 Hz), 7.07 (1H, d, J = 8.0 Hz), 7.19 (1H, d, J = 8.0 Hz), 7.41 (1H, t, J = 8.0 Hz), 8.04 (1H, d, J = 12.0 Hz), 8.34 (1H, d, J = 12.0 Hz), 9.66 (1H, s). ^{13}C NMR (100 MHz, $(CD_3)_2SO$)/δ (ppm): 40.3, 53.0, 105.8, 113.2, 115.5, 119.3, 121.6, 125.2, 128.4, 129.0, 130.8, 137.1, 137.7, 144.3, 145.5, 155.7, 165.6. HRMS Calcd for $C_{18}H_{17}N_2O_3$ $[M + H]^+$, 309.1239; found 309.1231

2-(((2-(Hydroxymethyl)quinolin-8-yl)amino)methyl)phenol (AQP4). A solution of (8-aminoquinolin-2-yl)methanol (**AQ4**) (100 mg, 0.574 mmol) was utilized to prepare **AQP4** following an identical procedure as the one described for **AQP2**. **AQP4** was purified by column chromatography (SiO_2, 1:1 EtOAc/Hx, R_f = 0.50) to yield the final product (light brown powder, 64.8 mg, 0.231 mmol, 40%). ^{1}H NMR (400 MHz, $(CD_3)_2SO$)/δ (ppm): 4.41 (2H, d, J = 8.0 Hz), 4.70 (2H, d, J = 8.0 Hz), 5.45 (1H, t, J = 8.0 Hz), 6.55 (1H, d, J = 8.0 Hz), 6.67 (1H, t, J = 8.0 Hz), 6.81 (1H, d, J = 8.0 Hz), 6.92 (1H, t, J = 8.0 Hz), 6.95−7.04 (2H, m), 7.16 (1H, d, J = 8.0 Hz), 7.22 (1H, t, J = 8.0 Hz), 7.53 (1H, d, J = 8.0 Hz), 8.15 (1H, d, J = 12.0 Hz), 9.56 (1H, s). ^{13}C NMR (100 MHz, $(CD_3)_2SO$)/δ (ppm): 41.9, 65.2, 105.2, 113.5, 115.4, 119.2, 119.6, 125.7, 127.5, 127.7, 128.1, 136.7, 136.9, 144.6, 155.6, 158.9. HRMS Calcd for $C_{17}H_{17}N_2O_2$ $[M + H]^+$, 281.1290; found 281.1280.

4-(Dimethylamino)-2-((quinolin-8-ylamino)methyl)phenol (AQDA1). To a solution of dry EtOAc (5.0 mL) was added quinolin-8-amine (**AQ1**) (100 mg, 0.694 mmol). 5-(Dimethylamino)-2-hydroxybenzaldehyde (**DHB**) (115 mg, 0.694 mmol) was slowly added to the reaction mixture. The reaction mixture was then protected from the light and allowed to stir overnight for 24 h. After 24 h, the reaction mixture was concentrated and dried. To a solution of DCE (5.0 mL) was added sodium triacetoxyborohydride (212 mg, 1.39 mmol). The sodium triacetoxyborohydride solution was then slowly added to the dried reaction mixture and allowed to stir for 24 h (protected from the light). After 24 h, the reaction mixture was concentrated and dissolved in dry methanol. Sodium borohydride (150 mg, 3.97 mmol) was added to the reaction mixture at 0 °C and allowed to stir for 2 h. After 2 h, the reaction mixture was quenched with sodium bicarbonate and H_2O, extracted with DCM (3×), and purified by column chromatography (SiO_2, 1:1 EtOAc/Hx, R_f = 0.43). The solid was recrystallized in DCM/Hx to afford the final product

DOI: 10.1021/acs.inorgchem.6b00525
Inorg. Chem. XXXX, XXX, XXX−XXX

(light brown powder, 140 mg, 0.479 mmol, 69%). ^{1}H NMR (400 MHz, $(CD_3)_2SO$)/δ (ppm): 2.63 (6H, s), 4.36 (2H, d, J = 4.0 Hz), 6.49 (1H, dd, J = 8.0 Hz, J = 4.0 Hz), 6.66−6.69 (2H, m), 6.74 (1H, d, J = 4.0 Hz), 6.79 (1H, t, J = 8.0 Hz), 7.01 (1H, d, J = 8.0 Hz), 7.29 (1H, t, J = 8.0 Hz), 7.46 (1H, dd, J = 8.0 Hz, J = 4.0 Hz), 8.16 (1H, dd, J = 6.8 Hz, J = 8.4 Hz), 8.69 (1H, dd, J = 2.4 Hz, J = 4.0 Hz), 8.83 (1H, s). ^{13}C NMR (100 MHz, $(CD_3)_2SO$)/δ (ppm): 41.8, 42.7, 105.2, 113.6, 113.7, 115.4, 116.0, 122.1, 125.9, 128.2, 128.7, 136.4, 138.0, 144.8 145.0, 147.3, 147.6. HRMS Calcd for $C_{18}H_{19}N_3NaO$ $[M + Na]^+$, 316.1426; found 316.1418.

4-(Dimethylamino)-2-(((2-methylquinolin-8-yl)amino)-methyl)phenol (AQDA2). A solution of 2-methylquinolin-8-amine (**AQ2**) (100 mg, 0.632 mmol) was utilized to prepare **AQDA2** following an identical procedure as the one described for **AQDA1**. **AQDA2** was purified by column chromatography (SiO_2, 1:3 EtOAc/Hx, R_f = 0.33). The solid was recrystallized in EtOAc/Hx to afford the final product (light brown powder, 83.5 mg, 0.272 mmol, 43%).^{1}H NMR (400 MHz, $(CD_3)_2SO$)/δ (ppm): 2.63 (3H, s), 2.68 (6H, s), 4.38 (2H, d, J = 8.0 Hz), 6.53 (1H, dd, J = 4.0 Hz, J = 8.0 Hz), 6.64 (1H, t, J = 8.0 Hz), 6.68−6.73 (2H, m), 6.77 (1H, d, J = 8.0 Hz), 7.00 (1H, d, J = 8.0 Hz), 7.25 (1H, t, J = 8.0 Hz), 7.36 (1H, d, J = 8.0 Hz), 8.07 (1H, d, J = 8.0 Hz), 8.86 (1H, s). ^{13}C NMR (100 MHz, $(CD_3)_2SO$)/δ (ppm): 25.3, 41.9, 43.0, 105.4, 113.6, 113.7, 115.4, 116.0, 122.6, 125.9, 126.7, 127.1, 136.6, 137.4, 144.5, 144.8, 147.6, 155.6. HRMS Calcd for $C_{19}H_{22}N_3O$ $[M + H]^+$, 308.1763; found 308.1762.

Methyl 8-((5-(dimethylamino)-2-hydroxybenzyl)amino)-quinoline-2-carboxylate (AQDA3). To a solution of dry EtOAc (15 mL) was added methyl 8-aminoquinoline-2-carboxylate (**AQ3**) (100 mg, 0.494 mmol). 5-(Dimethylamino)-2-hydroxybenzaldehyde (**DHB**) (82.6 mg, 0.494 mmol) was slowly added to the reaction mixture. The reaction mixture was then protected from the light and allowed to stir overnight for 24 h. After 24 h, the reaction mixture was concentrated and dried. To a solution of DCE (15 mL) was added sodium triacetoxyborohydride (209 mg, 0.988 mmol). The sodium triacetoxyborohydride solution was then slowly added to the dried reaction mixture and allowed to stir for 24 h (protected from the light). After 24 h, the reaction mixture was concentrated and purified by column chromatography (SiO_2, 1:1 EtOAc/Hx, R_f = 0.16). The solid was recrystallized in EtOAc/Hx to afford the final product (yellow powder, 111 mg, 0.316 mmol, 64%). ^{1}H NMR (400 MHz, $(CD_3)_2SO$)/δ (ppm): 2.69 (6H, s), 3.99 (3H, s), 4.43 (2H, d, J = 4.0 Hz), 6.55 (1H, dd, J = 9.0 Hz, J = 3.0 Hz), 6.71−6.82 (4H, m), 7.13 (1H, d, J = 8.0 Hz), 7.47 (1H, t, J = 8.0 Hz), 8.06 (1H, d, J = 8.0 Hz), 8.38 (1H, d, J = 9.0 Hz), 8.92 (1H, s). ^{13}C NMR (100 MHz, $(CD_3)_2SO$)/δ (ppm): 41.4, 42.4, 52.6, 105.6, 112.8, 113.4, 114.9, 115.7, 121.1, 124.9, 129.6, 130.4, 136.7, 137.2, 143.8, 144.3, 145.3, 147.2, 165.2. HRMS Calcd for $C_{20}H_{22}N_3O_3$ $[M + H]^+$, 352.1661; found 352.1658.

Aβ Aggregation Experiments. All experiments were performed according to previously published methods.[23,31,32,35] Prior to experiments, Aβ40 or Aβ42 was dissolved in ammonium hydroxide (NH_4OH, 1% v/v, aq), aliquoted, lyophilized overnight, and stored at −80 °C. For experiments described herein, a stock solution of Aβ was prepared by dissolving the lyophilized peptide in 1% NH_4OH (10 μL) and diluting with ddH_2O. The concentration of the solution was determined by measuring the absorbance of the solution at 280 nm (ε = 1450 M^{-1} cm^{-1} for Aβ40 and ε = 1490 M^{-1} cm^{-1} for Aβ42). The peptide stock solution was diluted to a final concentration of 25 μM in the Chelex-treated buffered solution containing HEPES [20 μM; pH 7.4 (for metal-free and Zn(II) samples) pH 6.6 (for Cu(II) samples) and NaCl (150 μM)]. For the inhibition studies,[23,31,32,35] compound (final concentration 50 μM, 1% v/v DMSO) was added to the sample of Aβ (25 μM) in the absence and presence of a metal chloride salt ($CuCl_2$ or $ZnCl_2$; 25 μM) followed by the incubation at 37 °C with constant agitation for 4, 8, and 24 h. For the disaggregation studies, Aβ with and without metal ions was incubated for 24 h at 37 °C with constant agitation prior to treatment with compound (50 μM). The resulting samples containing Aβ, a metal chloride salt, and a compound were incubated at 37 °C with constant agitation for 4, 8, and 24 h.

Gel Electrophoresis with Western Blotting. The samples from the inhibition and disaggregation experiments were analyzed by gel electrophoresis with Western blot using an anti-Aβ antibody (6E10).[23,31,32,35] Each sample (10 μL) was separated on a 10−20% Tris-tricine gel (Invitrogen, Grand Island, NY). Following separation, the proteins were transferred onto nitrocellulose, which was blocked with bovine serum albumin (BSA, 3% w/v, RMBIO, Missoula, MT) in Tris-buffered saline (TBS) containing 0.1% Tween-20 (TBS-T) for 4 h at room temperature. The membranes were incubated with antibody (6E10, 1:2000, Covance, Princeton, NJ) in a solution of 2% BSA (w/v in TBS-T) overnight at 4 °C. After washing, the horseradish peroxidase-conjugated goat antimouse secondary antibody (1:5000) in 2% BSA was added for 1 h at room temperature. ThermoScientific SuperSignal West Pico Chemiluminescent Substrate (Thermo Scientific, Rockford, IL), Biosesang ECL Plus kit (Biosesang, Gyeonggi-do, Republic of Korea), or a homemade ECL kit[41] was used to visualize the results on a ChemiDoc MP Imaging System (Bio-Rad, Hercules, CA).

Transmission Electron Microscopy (TEM). Samples for TEM were prepared according to previously reported methods.[23,31,32,35] Glow-discharged grids (Formar/Carbon 300-mesh, Electron Microscopy Sciences, Hatfield, PA) were treated with Aβ samples from the inhibition and disaggregation experiments (5 μL) for 2 min at room temperature. Excess sample was removed using filter paper followed by washing three times with ddH_2O. Each grid was incubated with uranyl acetate (1% w/v ddH_2O, 5 μL, 1 min). Upon removal of excess uranyl acetate with filter paper, the grids were dried for at least 30 min at room temperature before measurement. Images from each sample were taken on a JEOL JEM-2100 transmission electron microscope (UNIST Central Research Facilities, Ulsan National Institute of Science and Technology, Ulsan, Republic of Korea) at 120 kV and 25 000× magnification.

2D NMR Experiments. The interactions of Aβ40 monomer with **AQ** derivatives were interrogated by 2D band-selective optimized flip-angle short transient heteronuclear multiple quantum coherence (SOFAST-HMQC) NMR at 10 °C.[42] Uniformly ^{15}N-labeled Aβ40 (rPeptide, Bogart, GA) was dissolved in 1% NH_4OH and lyophilized to ensure the absence of preformed aggregates. The peptide was redissolved in 3 μL of DMSO-d_6 (Cambridge Isotope, Tewksbury, MA) and diluted by buffer to a final peptide concentration of 80 μM (20 mM PO_4, pH 7.4, 5 mM NaCl, 7% v/v D_2O). Each spectrum was obtained using 64 complex t_1 points and a 0.1 s recycle delay on a Bruker Avance 600 MHz spectrometer equipped with a cryoprobe. The data were processed using TOPSPIN 2.1 (Bruker), and assignment was performed using SPARKY 3.1134 using published assignments as a guide.[43−45] Chemical shift perturbation (CSP) was calculated using the following equation:

$$\Delta\delta_{NH} = \sqrt{\Delta\delta_H^2 + \left(\frac{\Delta\delta_N}{5}\right)^2}$$

Docking Studies. Flexible ligand docking studies for **AQ** derivatives against the Aβ40 monomer from a previously determined aqueous solution NMR structure (PDB 2LFM)[43] were conducted using AutoDock Vina.[46] Ten (10) conformations were selected from 20 conformations within the Protein Databank (PDB) file (1, 3, 5, 8, 10, 12, 13, 16, 17, and 20). The MMFF94 energy minimization in ChemBio3D Ultra 11.0 was used to optimize the ligand structures for docking studies. The structural files of the **AQ** derivatives and the peptide were generated by AutoDock Tools and imported into PyRx,[47] which were used to run AutoDock Vina.[46] The search space dimensions were set to contain the entire peptide. The exhaustiveness for the docking runs was set to 1024. Docked poses of the ligand with Aβ were visualized using Pymol.

Ion Mobility-Mass Spectrometry. All nanoelectrospray ionization MS (nESI-MS) combined with ion mobility-mass spectrometry (IM-MS) experiments were carried out on a Synapt G2 (Waters, Milford, MA).[48,49] Samples were ionized using a nanoelectrospray

DOI: 10.1021/acs.inorgchem.6b00525
Inorg. Chem. XXXX, XXX, XXX−XXX

source operated in positive ion mode. MS instrumentation was operated at a backing pressure of 2.7 mbar and sample cone voltage of 40 V. Aliquots of Aβ40 peptides (final concentration, 20 μM) were sonicated for 5 s prior to preincubation with or without a source of Cu(II) (copper(II) acetate, 20 μM) at 37 °C for 10 min. After preincubation, samples were titrated with or without ligand (**AQ1**, **AQ4**, **AQP1**, **AQP4**, **AQDA1−3**, or **ML**; final concentrations: 20, 40, 80, and 120 μM) and incubated at 37 °C for 30 min prior to analysis. Solution conditions were 100 mM ammonium acetate (pH 7.5) with 1% v/v DMSO. For control purposes, all data are compared to incubations of Aβ40 peptides with **EGCG** under the same conditions.[35] Collision cross-section (CCS) measurements were externally calibrated using a database of known values in helium, with values for proteins that bracket the likely CCS and ion mobility values of the unknown ions.[34,50] CCS values are the mean average of five replicates with errors reported as the least-squares product. This least-square analysis combines inherent calibrant error from drift tube measurements (3%),[50] calibration curve error, and twice the replicate standard deviation error. Determination of the amount of Cu(II) bound to Aβ40 was calculated using the total ion count extracted from the peak of interest at its full width half-maximum using methods previously described.[51] All other conditions are consistent with previously published methods.[32]

Metal Binding Experiments. Metal binding properties of **AQ1−3**, **AQP1−4**, and **AQDA1−3** were investigated by UV−vis and ^{1}H NMR. UV−vis experiments were carried out in acetonitrile (for **AQ2** and **AQP3**) or a Chelex-treated buffered solution containing 20 mM HEPES, pH 7.4, and 150 mM NaCl. To a solution of ligand, $CuCl_2$ or $ZnCl_2$ was titrated up to 10 equiv at room temperature. The solutions were allowed to equilibrate before further addition of $CuCl_2$ or $ZnCl_2$. Zn(II) binding to **AQ3** was probed by ^{1}H NMR by slowly titrating up to 3.5 equiv of $ZnCl_2$ (17.5 mM) at room temperature in CD_3CN. To examine the metal selectivity of **AQP4** and **AQDA1−3** for Cu(II), 1 or 20 equiv of $MgCl_2$, $CaCl_2$, $MnCl_2$, $FeCl_2$, $CoCl_2$, $NiCl_2$, and $ZnCl_2$ were first treated to a solution containing 50 μM ligand (**AQP4** and **AQDA1−3**). The spectra were recorded after 10 min incubation at room temperature. The Fe(II) samples were prepared in an anaerobic N_2-filled glovebox. $CuCl_2$ (50 μM) was then added to a solution of compound and a divalent metal chloride salt. The spectra were taken after an additional 10 min incubation period at room temperature. Quantification of metal selectivity was calculated by comparing and normalizing the absorption values of metal−ligand complexes at 290 (for **AQP4**), 440 (for **AQDA1** and **AQDA2**), and 338 nm (for **AQDA3**) to the absorption at these wavelengths before and after the addition of $CuCl_2$ (A_M/A_{Cu}).

Solution Speciation Studies. The pK_a values for **AQP1**, **AQP4**, and **AQDA1−3** were determined through UV−vis variable-pH titrations based on a previously reported procedure.[23,31,32,35] To obtain pK_a values for the ligands (50 μM for **AQP4** or **AQDA1**; 25 μM for **AQP1**, **AQDA2**, or **AQDA3**), HCl was titrated into the speciation solution (100 mM NaCl, pH 12, 10 mM NaOH) in small aliquots to obtain at least 30 spectra in the range pH 2−11 (for **AQP1** and **AQP4**) or pH 2−10 (for **AQDA1−3**). In addition, to investigate Cu(II) binding to the ligands at various pHs, small aliquots of HCl were titrated into the solutions containing a ligand and a metal chloride salt [[M(II)]:[L] = 1:2; [$CuCl_2$] = 50 (for **AQP4**), 12.5 (for **AQDA1** and **AQDA2**), and 25 μM (for **AQP1** and **AQDA3**)]. At least 30 spectra were measured over the range pH 2−8. The acidity and stability constants were calculated by using the HypSpec program (Protonic Software, Leeds, U.K.).[52,53]

2-Deoxyribose Assay. The ability of **AQ1**, **AQ3**, **AQ4**, **AQDA1**, and **AQDA3** to suppress the generation of hydroxyl radicals was determined by the 2-deoxyribose assay. The assay was preformed on the basis of previously reported methods.[23,36] Chelexed solutions were used, and reactions (total volume, 200 μL) were prepared by mixing, in the following order, buffer (50 mM NaH_2PO_4, pH 7.4), ligand (125 μM), $CuCl_2$ (10 μM), 2-deoxy-D-ribose (15 mM), H_2O_2 (200 μM), and sodium ascorbate (2 mM) and allowed to react for 1 h at 37 °C with constant agitation. The reactions were quenched upon addition of trichloroacetic acid (200 μL of 2.8% m/v) and 2-thiobarbituric acid (200 μL of 1% w/v). After quenching, the reactions were heated at 100 °C for 20 min, and then allowed to cool for 5 min prior to measurement of their absorbance values at 532 nm. Samples without ligand were prepared as a control. Experiments were preformed in triplicate. Normalized absorbance values (A/A_0) were calculated by taking the absorbance (A) and dividing by the absorbance of the control (A_0).

Trolox Equivalent Antioxidant Capacity (TEAC) Assay. The antioxidant activity of **AQ1−3**, **AQP1−2**, **AQP4**, and **AQDA1−3** was determined by the TEAC assay using human neuroblastoma SK-N-BE(2)-M17 (M17) cell lysates and was conducted according to a protocol of the antioxidant assay kits purchased from Cayman Chemical Company (Ann Arbor, MI) with minor modifications. The cell line purchased from ATCC (Manassas, VA) was maintained in media containing 1:1 minimum Essential Media (MEM, GIBCO) and Ham's F12K Kaighn's Modification Media (F12K, GIBCO), 10% (v/v) fetal bovine serum (FBS, GIBCO), 100 U/mL penicillin (GIBCO), and 100 mg/mL streptomycin (GIBCO). The cells were grown and maintained at 37 °C in a humidified atmosphere with 5% CO_2. The cells were seeded in a 6 well plate and grown to approximately 80−90% confluence. Cell lysates were prepared following a previously reported method with modifications.[54] M17 cells were washed once with cold PBS (pH 7.4, GIBCO) and harvested by gently pipetting off adherent cells with cold PBS. A cell pellet was generated by centrifugation (2000 g for 10 min at 4 °C). This cell pellet was sonicated on ice (5 s pulses five times with 20 s intervals between each pulse) in 2 mL of cold Assay Buffer [5 mM potassium phosphate (pH 7.4) containing 0.9% NaCl and 0.1% glucose]. The cell lysates were centrifuged at 10 000 g for 10 min at 4 °C. The supernatant was removed and stored on ice until use. To a standard sample 96 microplate, 10 μL of the supernatant cell lysates was delivered followed by addition of compound, metmyoglobin (2.5 μM), ABTS (165 μM), and H_2O_2 (82.4 μM) in order. Compound concentration ranges utilized were as follows: Trolox (45, 90, 135, 180, 225, and 330 μM); **AQ1**, **AQ3**, **AQP4**, **AQDA1**, and **AQDA2** (30, 50, 70, 90, 110, and 135 μM); **AQ2** (30, 70, 110, 150, 190, and 255 μM); **AQP1** and **AQP2** (20, 40, 60, 80, 100, and 120 μM); **AQDA3** (30, 60, 90, 120, 150, and 180 μM). After 5 min incubation at room temperature on a shaker, absorbance values at 750 nm were recorded. The percent inhibition was calculated according to the measured absorbance (% inhibition = $(A_0 - A)/A_0$, where A_0 is the absorbance of the supernatant of cell lysates) and was plotted as a function of compound concentration. The TEAC value of ligands was calculated as a ratio of the slope of the standard curve of the compound to that of Trolox. The measurements were conducted in triplicate.

Parallel Artificial Membrane Permeability Adapted for the Blood−Brain Barrier (PAMPA-BBB) Assay. PAMPA-BBB experiments were carried out using the PAMPA Explorer kit (*p*ION Inc., Billerica, MA) with modifications to previously reported protocols.[23,25,26,55] Each stock solution was diluted with Prisma HT buffer (pH 7.4, *p*ION) to a final concentration of 25 μM (1% v/v final DMSO concentration). The resulting solution was added to wells of the donor plate (200 μL, 12 replicates). BBB-1 lipid formulation (5 μL, *p*ION) was used to coat the polyvinylidene fluoride (PVDF, 0.45 mM) filter membrane on the acceptor plate. This acceptor plate was placed on top of the donor plate forming a sandwich. Brain sink buffer (BSB, 200 μL, *p*ION) was added to each well of the acceptor plate. The sandwich was incubated for 4 h at ambient temperature without stirring. UV−vis spectra of the solutions in the reference, acceptor, and donor plates were measured using a microplate reader. The PAMPA Explorer software v. 3.5 (*p*ION) was used to calculate $-\log P_e$ for each compound. CNS± designations were assigned by comparison to compounds that were identified in previous reports.[25,26,55]

Cell Viability Measurements. The mouse Neuro-2a (N2a) neuroblastoma cell line was purchased from the American Type Cell Collection (ATCC, Manassas, VA). Cells were maintained in media containing 1:1 DMEM (GIBCO, Grand Island, NY) and opti-MEM (GIBCO), supplemented with 5% (v/v) fetal bovine serum (FBS; GIBCO), 1% (v/v) L-glutamine (GIBCO), 100 U/mL penicillin, and 100 mg/mL streptomycin (GIBCO). The cells were grown and

DOI: 10.1021/acs.inorgchem.6b00525
Inorg. Chem. XXXX, XXX, XXX−XXX

maintained at 37 °C in a humidified atmosphere with 5% CO_2. Cell viability upon treatment with compounds was determined by the MTT assay [MTT = 3-(4,5-dimethyl-2-thiazolyl)-2,5-diphenyl-2*H*-tetrazolium bromide, Sigma-Aldrich]. N2a cells were seeded in a 96 well plate (15 000 cells in 100 μL per well). The cells were treated with compounds (5 or 10 μM, 1% v/v final DMSO concentration) with or without $CuCl_2$ or $ZnCl_2$ (5 or 10 μM), and incubated for 24 h. After incubation, MTT [25 μL; 5 mg/mL in phosphate buffered saline (PBS, pH 7.4, GIBCO)] was added to each well, and the plate was incubated for 4 h at 37 °C. Formazan produced by the cells was solubilized using an acidic solution of *N*,*N*-dimethylformamide (DMF, 50%, v/v aq) and sodium dodecyl sulfate (SDS, 20%, w/v) overnight at room temperature in the dark. The absorbance was measured at 600 nm using a microplate reader. Cell viability was calculated relative to cells treated with an equivalent amount of DMSO. All experiments were performed in triplicate.

■ ASSOCIATED CONTENT

Supporting Information

The Supporting Information is available free of charge on the ACS Publications website at DOI: 10.1021/acs.inorgchem.6b00525.

Syntheses, docking investigations, cytotoxicity investigations, additional gel/Western blot, TEM, NMR, mass spectrometry, and metal binding experiments (PDF)

■ AUTHOR INFORMATION

Corresponding Author

*E-mail: mhlim@unist.ac.kr.

Notes

The authors declare no competing financial interest.

■ ACKNOWLEDGMENTS

This work was supported by the University of Michigan Protein Folding Disease Initiative (to A.R., B.T.R., and M.H.L.) and the National Research Foundation of Korea (NRF) grant funded by the Korean government [NRF-2014S1A2A2028270 (to M.H.L. and A.R.); NRF-2014R1A2A2A01004877 (to M.H.L.)], and the 2016 Research Fund (Project Number 1.160001.01) of Ulsan National Institute of Science and Technology (UNIST). J.K. acknowledges the support from the Global Ph.D. fellowship program through the National Research Foundation of Korea (NRF) funded by the Ministry of Education (NRF-2015HIA2A1030823).

■ REFERENCES

(1) Guzior, N.; Wieckowska, A.; Panek, D.; Malawska, B. *Curr. Med. Chem.* **2015**, *22*, 373−404.
(2) Perez, L. R.; Franz, K. J. *Dalton Trans.* **2010**, *39*, 2177−2187.
(3) Zatta, P.; Drago, D.; Bolognin, S.; Sensi, S. L. *Trends Pharmacol. Sci.* **2009**, *30*, 346−355.
(4) Duce, J. A.; Bush, A. I. *Prog. Neurobiol.* **2010**, *92*, 1−18.
(5) Haass, C.; Selkoe, D. J. *Nat. Rev. Mol. Cell Biol.* **2007**, *8*, 101−112.
(6) Jakob-Roetne, R.; Jacobsen, H. *Angew. Chem., Int. Ed.* **2009**, *48*, 3030−3059.
(7) Scott, L. E.; Orvig, C. *Chem. Rev.* **2009**, *109*, 4885−4910.
(8) Miller, Y.; Ma, B.; Nussinov, R. *Chem. Rev.* **2010**, *110*, 4820−4838.
(9) Telpoukhovskaia, M. A.; Orvig, C. *Chem. Soc. Rev.* **2013**, *42*, 1836−1846.
(10) Jensen, M.; Canning, A.; Chiha, S.; Bouquerel, P.; Pedersen, J. T.; Østergaard, J.; Cuvillier, O.; Sasaki, I.; Hureau, C.; Faller, P. *Chem. - Eur. J.* **2012**, *18*, 4836−4839.
(11) Kepp, K. P. *Chem. Rev.* **2012**, *112*, 5193−5239.
(12) Derrick, J. S.; Lim, M. H. *ChemBioChem* **2015**, *16*, 887−898.
(13) Corbett, A.; Pickett, J.; Burns, A.; Corcoran, J.; Dunnett, S. B.; Edison, P.; Hagan, J. J.; Holmes, C.; Jones, E.; Katona, C.; Kearns, I.; Kehoe, P.; Mudher, A.; Passmore, A.; Shepherd, N.; Walsh, F.; Ballard, C. *Nat. Rev. Drug Discovery* **2012**, *11*, 833−846.
(14) Rodríguez-Rodríguez, C.; Telpoukhovskaia, M.; Orvig, C. *Coord. Chem. Rev.* **2012**, *256*, 2308−2332.
(15) Schugar, H.; Green, D. E.; Bowen, M. L.; Scott, L. E.; Storr, T.; Böhmerle, K.; Thomas, F.; Allen, D. D.; Lockman, P. R.; Merkel, M.; Thompson, K. H.; Orvig, C. *Angew. Chem., Int. Ed.* **2007**, *46*, 1716−1718.
(16) Lincoln, K. M.; Offutt, M. E.; Hayden, T. D.; Saunders, R. E.; Green, K. N. *Inorg. Chem.* **2014**, *53*, 1406−1416.
(17) Lincoln, K. M.; Gonzalez, P.; Richardson, T. E.; Julovich, D. A.; Saunders, R.; Simpkins, J. W.; Green, K. N. *Chem. Commun.* **2013**, *49*, 2712−2714.
(18) Lincoln, K. M.; Richardson, T. E.; Rutter, L.; Gonzalez, P.; Simpkins, J. W.; Green, K. N. *ACS Chem. Neurosci.* **2012**, *3*, 919−927.
(19) Otto, R.; Penzis, R.; Gaube, F.; Adolph, O.; Föhr, K. J.; Warncke, P.; Robaa, D.; Appenroth, D.; Fleck, C.; Enzensperger, C.; Lehmann, J.; Winckler, T. *J. Med. Chem.* **2015**, *58*, 6710−6715.
(20) Telpoukhovskaia, M. A.; Cawthray, J. F.; Rodríguez-Rodríguez, C.; Scott, L. E.; Page, B. D. G.; Patrick, B. O.; Orvig, C. *Bioorg. Med. Chem. Lett.* **2015**, *25*, 3654−3657.
(21) Storr, T.; Merkel, M.; Song-Zhao, G. X.; Scott, L. E.; Green, D. E.; Bowen, M. L.; Thompson, K. H.; Patrick, B. O.; Schugar, H. J.; Orvig, C. *J. Am. Chem. Soc.* **2007**, *129*, 7453−7463.
(22) Wang, Z.; Wang, Y.; Li, W.; Mao, F.; Sun, Y.; Huang, L.; Li, X. *ACS Chem. Neurosci.* **2014**, *5*, 952−962.
(23) Lee, S.; Zheng, X.; Krishnamoorthy, J.; Savelieff, M. G.; Park, H. M.; Brender, J. R.; Kim, J. H.; Derrick, J. S.; Kochi, A.; Lee, H. J.; Kim, C.; Ramamoorthy, A.; Bowers, M. T.; Lim, M. H. *J. Am. Chem. Soc.* **2014**, *136*, 299−310.
(24) Savelieff, M. G.; DeToma, A. S.; Derrick, J. S.; Lim, M. H. *Acc. Chem. Res.* **2014**, *47*, 2475−2482.
(25) Di, L.; Kerns, E. H.; Fan, K.; McConnell, O. J.; Carter, G. T. *Eur. J. Med. Chem.* **2003**, *38*, 223−232.
(26) Avdeef, A.; Bendels, S.; Di, L.; Faller, B.; Kansy, M.; Sugano, K.; Yamauchi, Y. *J. Pharm. Sci.* **2007**, *96*, 2893−2909.
(27) Lim, M. H.; Wong, B. A.; Pitcock, W. H.; Mokshagundam, D.; Baik, M.-H.; Lippard, S. J. *J. Am. Chem. Soc.* **2006**, *128*, 14364−14373.
(28) Waibel, M.; Hasserodt, J. *Tetrahedron Lett.* **2009**, *50*, 2767−2769.
(29) Roth, R.; Erlenmeyer, H. *Helv. Chim. Acta* **1954**, *37*, 1064−1068.
(30) Shaffer, K. J.; Davidson, R. J.; Burrell, A. K.; McCleskey, T. M.; Plieger, P. G. *Inorg. Chem.* **2013**, *52*, 3969−3975.
(31) Derrick, J. S.; Kerr, R. A.; Nam, Y.; Oh, S. B.; Lee, H. J.; Earnest, K. G.; Suh, N.; Peck, K. L.; Ozbil, M.; Korshavn, K. J.; Ramamoorthy, A.; Prabhakar, R.; Merino, E. J.; Shearer, J.; Lee, J.-Y.; Ruotolo, B. T.; Lim, M. H. *J. Am. Chem. Soc.* **2015**, *137*, 14785−14797.
(32) Beck, M. W.; Oh, S. B.; Kerr, R. A.; Lee, H. J.; Kim, S. H.; Kim, S.; Jang, M.; Ruotolo, B. T.; Lee, J.-Y.; Lim, M. H. *Chem. Sci.* **2015**, *6*, 1879−1886.
(33) Hernández, H.; Robinson, C. V. *Nat. Protoc.* **2007**, *2*, 715−726.
(34) Ruotolo, B. T.; Benesch, J. L. P.; Sandercock, A. M.; Hyung, S.-J.; Robinson, C. V. *Nat. Protoc.* **2008**, *3*, 1139−1152.
(35) Hyung, S.-J.; DeToma, A. S.; Brender, J. R.; Lee, S.; Vivekanandan, S.; Kochi, A.; Choi, J.-S.; Ramamoorthy, A.; Ruotolo, B. T.; Lim, M. H. *Proc. Natl. Acad. Sci. U. S. A.* **2013**, *110*, 3743−3748.
(36) Charkoudian, L. K.; Pham, D. M.; Franz, K. J. *J. Am. Chem. Soc.* **2006**, *128*, 12424−12425.
(37) Re, R.; Pellegrini, N.; Proteggente, A.; Pannala, A.; Yang, M.; Rice-Evans, C. *Free Radical Biol. Med.* **1999**, *26*, 1231−1237.
(38) Puskullu, M. O.; Tekiner, B.; Süzen, S. *Mini-Rev. Med. Chem.* **2013**, *13*, 365−372.
(39) Havsteen, B. H. *Pharmacol. Ther.* **2002**, *96*, 67−202.
(40) Rice-Evans, C.; Miller, N. J.; Paganga, G. *Free Radical Biol. Med.* **1996**, *20*, 933−956.
(41) Mruk, D. D.; Cheng, C. Y. *Spermatogenesis* **2011**, *1*, 121−122.

DOI: 10.1021/acs.inorgchem.6b00525
Inorg. Chem. XXXX, XXX, XXX−XXX

(42) Schanda, P.; Brutscher, B. *J. Am. Chem. Soc.* **2005**, *127*, 8014−8015.
(43) Vivekanandan, S.; Brender, J. R.; Lee, S. Y.; Ramamoorthy, A. *Biochem. Biophys. Res. Commun.* **2011**, *411*, 312−316.
(44) Yoo, S. I.; Yang, M.; Brender, J. R.; Vivekanandan, S.; Sun, K.; Joo, N. E.; Jeong, S.-H.; Ramamoorthy, A.; Kotov, N. A. *Angew. Chem., Int. Ed.* **2011**, *50*, 5110−5115.
(45) Fawzi, N. L.; Ying, J.; Torchia, D. A.; Clore, G. M. *J. Am. Chem. Soc.* **2010**, *132*, 9948−9951.
(46) Trott, O.; Olson, A. J. *J. Comput. Chem.* **2010**, *31*, 455−461.
(47) Wolf, C. K. *Chem. Eng. News* **2009**, *87*, 31.
(48) Giles, K.; Williams, J. P.; Campuzano, I. *Rapid Commun. Mass Spectrom.* **2011**, *25*, 1559−1566.
(49) Zhong, Y.; Hyung, S.-J.; Ruotolo, B. T. *Analyst* **2011**, *136*, 3534−3541.
(50) Bush, M. F.; Hall, Z.; Giles, K.; Hoyes, J.; Robinson, C. V.; Ruotolo, B. T. *Anal. Chem.* **2010**, *82*, 9557−9565.
(51) Soper, M. T.; DeToma, A. S.; Hyung, S.-J.; Lim, M. H.; Ruotolo, B. T. *Phys. Chem. Chem. Phys.* **2013**, *15*, 8952−8961.
(52) Gans, P.; Sabatini, A.; Vacca, A. *Ann. Chim.* **1999**, *89*, 45−49.
(53) Alderighi, L.; Gans, P.; Ienco, A.; Peters, D.; Sabatini, A.; Vacca, A. *Coord. Chem. Rev.* **1999**, *184*, 311−318.
(54) Spencer, V. A.; Sun, J.-M.; Li, L.; Davie, J. R. *Methods* **2003**, *31*, 67−75.
(55) *BBB Protocol and Test Compounds*; pION Inc.: Woburn, MA, 2009.

DOI: 10.1021/acs.inorgchem.6b00525
Inorg. Chem. XXXX, XXX, XXX−XXX